Title

Design and Optimization of Anti-amyloid Domain Antibodies Specific for β-Amyloid and Islet Amyloid Polypeptide*

Journal

Journal of Biological Chemistry, 291(6)

ISSN

0021-9258

Authors

Lee, Christine C
Julian, Mark C
Tiller, Kathryn E
et al.

Publication Date

2016-02-01

DOI

10.1074/jbc.m115.682336

THE JOURNAL OF BIOLOGICAL CHEMISTRY VOL. 291, NO. 6, pp. 2858–2873, February 5, 2016

Design and Optimization of Anti-amyloid Domain Antibodies Specific for β-Amyloid and Islet Amyloid Polypeptide*

Received for publication, August 5, 2015, and in revised form, November 18, 2015 Published, JBC Papers in Press, November 24, 2015, DOI 10.1074/jbc.M115.682336

Christine C. Lee[‡], Mark C. Julian[‡], Kathryn E. Tiller[‡], Fanling Meng[‡], Sarah E. DuConge[‡], Rehana Akter[§], Daniel P. Raleigh[§], and Peter M. Tessier[‡1]

From the [‡]Center for Biotechnology and Interdisciplinary Studies, Isermann Department of Chemical and Biological Engineering, Rensselaer Polytechnic Institute, Troy, New York 12180 and the [§]Department of Chemistry, Stony Brook University, Stony Brook, New York 11794

Antibodies with conformational specificity are important for detecting and interfering with polypeptide aggregation linked to several human disorders. We are developing a motif-grafting approach for designing lead antibody candidates specific for amyloid-forming polypeptides such as the Alzheimer peptide (Aβ). This approach involves grafting amyloidogenic peptide segments into the complementarity-determining regions (CDRs) of single-domain (V_H) antibodies. Here we have investigated the impact of polar mutations inserted at the edges of a large hydrophobic Aβ42 peptide segment (Aβ residues 17–42) in CDR3 on the solubility and conformational specificity of the corresponding V_H domains. We find that V_H expression and solubility are strongly enhanced by introducing multiple negatively charged or asparagine residues at the edges of CDR3, whereas other polar mutations are less effective (glutamine and serine) or ineffective (threonine, lysine, and arginine). Moreover, Aβ V_H domains with negatively charged CDR3 mutations show significant preference for recognizing Aβ fibrils relative to Aβ monomers, whereas the same V_H domains with other polar CDR3 mutations recognize both Aβ conformers. We observe similar behavior for a V_H domain grafted with a large hydrophobic peptide from islet amyloid polypeptide (residues 8–37) that contains negatively charged mutations at the edges of CDR3. These findings highlight the sensitivity of antibody binding and solubility to residues at the edges of CDRs, and provide guidelines for designing other grafted antibody fragments with hydrophobic binding loops.

The misfolding and assembly of peptides and proteins into prefibrillar oligomers and amyloid fibrils is linked to several neurodegenerative diseases (1–4). To understand the contributions of polypeptide aggregation to such disorders, it is important to characterize the biochemical properties of aggregates. However, pre-amyloid and amyloid aggregates are difficult to characterize using many traditional biochemical methods that are routinely used for soluble proteins. High-resolution structural analysis of such aggregates is particularly challenging and must be performed using specialized methods such as solid state NMR (5–13) or x-ray crystallography of small peptide fragments (14–16). These powerful structural methods generally lack the time resolution to probe pre-amyloid intermediates and oligomers unless they can be kinetically trapped.

Given these challenges, antibodies with conformational specificity for prefibrillar oligomers and amyloid fibrils have proven valuable for biochemical characterization (17–28). An obvious strength of such antibodies is their ability to detect specific types of aggregates formed both *in vivo* and *in vitro*. The ability of conformational antibodies to bridge *in vivo* and *in vitro* studies is important for understanding the biochemical mechanisms that contribute to protein misfolding disorders.

Several approaches have been used to generate conformational antibodies. The most widely used one is immunization, which has yielded a wide range of important antibodies specific for different types of prefibrillar oligomers and amyloid fibrils (17–20, 25–27). Another powerful approach that has proven useful is to employ *in vitro* display methods such as phage and yeast surface display (21–24, 29–37). These display methods afford more control over antigen presentation and have been used primarily to identify antibody fragments (rather than full-length antibodies) specific for oligomers and fibrils of several amyloid-forming polypeptides.

Nevertheless, it remains a challenge to generate antibodies with sequence and conformational specificity for different types of amyloid aggregates, which is required for many applications. To address this challenge, we are investigating the potential of designing conformational antibody fragments by mimicking the natural process of amyloid formation (38). Our approach is to graft amyloidogenic peptide segments from polypeptides such as the Alzheimer Aβ[2] peptide into the complementarity-determining regions (CDRs) of single-domain (V_H) antibodies. We find that these Grafted AMyloid-Motif AntiBODIES (gammabodies) recognize their cognate amyloid

* This work was supported, in whole or in part, by National Institutes of Health Grants R01GM104130 (to P. M. T.) and R01GM078114 (to D. P. R.), National Science Foundation CBET Grants 0954450 and 1159943 (to P. M. T.), grants from the Pew Charitable Trust (Pew Scholars Award in Biomedical Sciences (to P. M. T.), New York Capital Region Research Alliance (to P. M. T.), and Richard Baruch M.D. Chair (to P. M. T). P.M.T. has received consulting fees and/or honorariums for presentations of this and/or related research findings at MedImmune, Eli Lilly, Bristol-Myers Squibb, Janssen, Merck, Genentech, Amgen, Pfizer, Adimab, Abbvie, Roche, Boehringer Ingelheim, Bayer, Abbott, DuPont, Schrödinger, and Novo Nordisk. The content is solely the responsibility of the authors and does not necessarily represent the official views of the National Institutes of Health.

[1] To whom correspondence should be addressed. Tel.: 518-276-2045; E-mail: tessier@rpi.edu.

[2] The abbreviations used are: Aβ, amyloid β; V_H, variable domain of heavy chain; IAPP, islet amyloid polypeptide; T_m, melting temperature; ThT, thioflavin T; CDR, complementarity-determining region; PrP, prion protein; Bis-Tris, 2-[bis(2-hydroxyethyl)amino]-2-(hydroxymethyl)propane-1,3-diol; RCF, relative centrifugal force; GuHCl, guanidine hydrochloride.

aggregates via homotypic interactions with modest (submicromolar to micromolar) affinity, and weakly recognize disaggregated conformers as well as amyloid aggregates formed by other polypeptides (38–40).

The Alzheimer Aβ peptide contains two key amyloidogenic peptide segments that mediate aggregation and are structured within the amyloid core (6, 7, 41, 42). In the more amyloidogenic variant of Aβ (Aβ42), these segments typically include residues ^{17}LVFFA^{21} and ^{31}IIGLMVGGVVIA^{42}. We posited that a V_H antibody grafted with an Aβ peptide fragment containing both segments (Aβ residues 17–42) would have improved binding properties relative to shorter 10-mer variants that we have previously reported (38–40). Moreover, our previous results (39, 40) suggested that adding hydrophilic residues to the edges of CDR3 would enhance the solubility of V_H domains displaying this large amyloidogenic peptide. We also posited that these flanking polar residues would influence the conformational specificity of the Aβ V_H domains as well. Therefore, we have investigated the solubility and conformational specificity of Aβ17–42 V_H domains with different hydrophilic residues inserted at the edges of CDR3. We have also evaluated the generality of these findings by applying them to design antibody domains specific for islet amyloid polypeptide (IAPP), which is the polypeptide responsible for amyloid formation in type 2 diabetes.

Experimental Procedures

Antibody Engineering, Expression, and Purification—Genes for V_H expression were created using polymerase chain reaction-based gene synthesis (43) and ligated into a pET-17b bacterial expression vector (Novagen) between the NdeI and XhoI restriction sites. Restriction sites for BamHI and NotI were inserted at the edges of the CDR3 loop for introducing different sequences via ligation of synthetic primers. A PelB leader sequence was added to the N terminus of the V_H gene to direct it to the periplasm. A triple FLAG tag was added to the C terminus of the V_H domain, followed by a His_7 tag.

Vectors containing the V_H gene were transformed into BL21(DE3) pLysS cells (200132, Agilent Technologies). Transformed cells were incubated on LB-ampicillin plates for 2 days at room temperature. Next, V_H expression was performed for 48 h at 20 °C and 225 rpm in 1-liter shaker flasks containing 200 ml of autoinduction media (44) supplemented with ampicillin (100 μg/ml) and chloramphenicol (35 μg/ml). Cells were sedimented by centrifugation and then discarded. Nickel-agarose resin (30230, Qiagen) was added to the clarified supernatant and incubated overnight.

The protein of interest was isolated by batch purification. The resin was washed with 100 mM imidazole at pH 7.4 to remove impurities, prior to elution with 250 mM imidazole at pH 7.4. Eluted samples were then refolded by denaturation in 6 M GuHCl at pH 7.4. Following an overnight incubation, the samples were then refolded at 4 °C by buffer exchanging into PBS, filtered, and stored at −80 °C. Refolded samples were analyzed via SDS-PAGE (WG1203BX10, Life Technologies) for samples that were reduced and boiled. The gels were then stained using Coomassie dye (24615, Thermo Scientific). The concentration of the V_H domains was measured using a Bradford assay (1856209, Thermo Fisher Scientific).

Expression of V_H Domains in Pichia pastoris—V_H domains were also expressed in *P. pastoris*. The V_H genes were inserted into the pJ912 *Pichia* expression vector (DNA2.0, Inc.), which was linearized at the SacI restriction site to direct integration of the plasmid into chromosomal DNA at the AOX1 promoter. Cells were transformed by electroporation and then grown on plates (yeast extract peptone dextrose medium with sorbitol) supplemented with 1 mg/ml of zeocin. Colonies were picked and grown overnight in a 5-ml seed culture at 30 °C and 225 rpm. The seed cultures were then added to baffled shake flasks with 50 ml of minimal media containing glucose. The cells were grown for 60 h at 30 °C and 225 rpm, and then induced with methanol (0.5% final concentration). Expression of V_H domains was detected in supernatant samples via SDS-PAGE (WG1203BX10, Life Technologies) and silver staining (LC6100, Life Technologies).

Yeast Surface Display Analysis of Aga2-V_H Fusions—Yeast surface display was performed with the EBY100 *Saccharomyces cerevisiae* strain using methods that we have described previously (45). Aga2-V_H fusions were subcloned from existing pET-17b constructs using PCR amplification to introduce overhangs complementary to the pCTCON2 yeast display plasmid. The PCR products were mixed with pCTCON2 plasmid that was digested with NheI and SalI, and transformed into the EBY100 strain for homologous recombination and selection on SD-CAA agar plates.

Overnight yeast cell cultures were miniprepped (D2004, Zymoprep II yeast miniprep kit, Zymo Research) and subsequently transformed into electroporation competent XL1-blue bacterial cells (200228, Agilent Technologies). Individual bacterial colonies were miniprepped (27106, Qiagen) and sequenced. Cells were then transformed with pCTCON2 plasmids encoding Aga2-V_H fusions and grown overnight at 30 °C with agitation in low pH SD-CAA medium (20 g/liter of dextrose, 6.7 g/liter of yeast nitrogen base, 5 g/liter of casamino acids, 14.7 g/liter of sodium citrate, and 4.3 g/liter of citric acid) to an A_{600} of 1–2. Surface display of the Aga2-V_H fusions was induced by pelleting the cells and resuspending them in SG-CAA media (20 g/liter of galactose, 6.7 g/liter of yeast nitrogen base, 5 g/liter of casamino acids, 8.56 g/liter of $NaH_2PO_4{\cdot}H_2O$, and 5.4 g/liter of $Na_2HPO_4{\cdot}2H_2O$). The cells were then incubated overnight at 30 °C with agitation. Both the SD-CAA and SG-CAA media were supplemented with 100 μg/ml of ampicillin and kanamycin as well as a 1× solution of penicillin/streptomycin.

Display levels were analyzed using flow cytometry. For each Aga2-V_H fusion, ~10^6 cells were collected and washed twice with 1 ml of PBS-BX (PBS with 10 mg/ml of BSA and 1% (v/v) Triton X-100). A C-terminal epitope (myc) tag was then probed with anti-myc IgY antibody (1:200 dilution; A-21280, Life Technologies) for 1–5 h at 25 °C. After this incubation, the cells were washed with 1 ml of PBS-BX before labeling with a secondary antibody (1:100 dilution, Alexa Fluor 488-conjugated goat anti-chicken IgG, A-11039, Life Technologies) for 5 min. Fluorescently labeled cells were washed again in 1 ml of PBS-BX and the level of Aga2-V_H display (as judged using the anti-myc

antibody) was analyzed on a BD LSRII flow cytometer using 100,000 events.

Circular Dichroism Analysis—The secondary structure of V_H domains was characterized by collecting their circular dichroism (CD) spectra on a Jasco J-815 spectrometer in the far-UV region of 200–260 nm. Samples were diluted to 0.2 g/liter in PBS, and their spectra were measured using a cuvette with a 1-mm path length. Scans were collected at a rate of 50 nm/min (1 nm bandwidth and 4 s response time). For each V_H domain, 10 spectra were collected and averaged. Mean residue ellipticity values were calculated from the background-subtracted spectra.

For each V_H domain, the reversibility of unfolding after thermal denaturation was monitored by CD. V_H domains were diluted to 0.1 g/liter in PBS in a cuvette with a 1-cm path length. Samples were heated from 25 to 95 °C at a rate of 1 °C/min, while monitoring the ellipticity at 235 nm. Following the first melt, samples were cooled to 25 °C for at least 20 min before repeating the melt. The fraction of V_H domain that remained folded over the course of the melt was calculated as $(\theta_T - \theta_U)/(\theta_F - \theta_U)$. θ_T is the ellipticity signal as a function of temperature, and θ_U and θ_F are the ellipticity signals for the unfolded and folded samples, respectively. The apparent melting temperature (T_m) was calculated from the initial melt.

Protein A Binding Assay—The binding of V_H domains to Protein A was measured in well plates using immobilized Protein A. Recombinant Protein A (77673, Pierce) was diluted to 5 μM in PBS, and 100 μl was added to a Nunc-Immuno 96-well plate with MaxiSorp surface coating (442404, Thermo Fisher Scientific). Protein A was incubated in the plate at room temperature overnight. Milk was then added to the plate at a concentration of 10% (w/v) and incubated at room temperature for several hours. The plate was then washed with PBS, and V_H domains at varying concentrations in PBST (PBS with 0.1% (v/v) Tween 20) were added (100 μl).

The V_H domains were incubated in the wells overnight at room temperature. The plate was then washed with PBS, and 100 μl of monoclonal anti-FLAG tag antibody produced in mouse (F1804-1 mg, Sigma) was added that had been diluted 1000-fold in PBST. Following a 1 h incubation of the anti-FLAG antibody, the plate was washed again with PBS, and 100 μl of an HRP-conjugated goat anti-mouse secondary antibody (32430, Pierce) was added that had been diluted 1000-fold in PBST. After 1 h of incubation, the plate was washed a final time with PBS, and 100 μl of substrate (1-Step Ultra TMB-ELISA Substrate Solution, 34028, Life Technologies) was added. The plates were developed for 1 h, and the reaction quenched by adding 2 M H_2SO_4 (100 μl). Signals were determined by measuring the absorbance at 450 nm for each well using a Tecan Safire^2 plate reader. IC_{50} values were calculated from the dose-response curve that was generated for each V_H domain.

Antibody Solubility Analysis—The relative solubility of V_H domains as a function of temperature was analyzed. Samples were diluted to ~13 μM in PBS, and divided into multiple aliquots. Each aliquot was held at a given temperature (50–95 °C) for 20 min, and then cooled to room temperature. The concentration of protein remaining in solution was measured by first centrifuging the cooled sample for 15 min at 21,000 RCF. Afterward, the top 50% of the supernatant volume was removed to determine the soluble V_H concentration using the Bradford assay.

The relative solubility of V_H domains at 25 °C was also analyzed by monitoring their monomeric content over a week. Samples were prepared by centrifuging them at 208,000 RCF for 1 h at 4 °C, and then recovering the top 80% of the supernatant. This procedure aimed to remove aggregated species at the beginning of the experiment. The samples were then concentrated to ~1 g/liter (~50 μM) using ultracentrifugal concentrators (10-kDa molecular weight cut-off membrane, UFC501096, Millipore). The monomeric content of the initial and 1 week samples was analyzed by size exclusion chromatography. A Waters 600F HPLC instrument was used to inject 10 μl of sample at ~1 g/liter onto a TSKgel G3000SW$_{XL}$ column (08541, Tosoh Bioscience) with an in-line guard column (08543, Tosoh Bioscience). The mobile phase was PBS with 0.2 M arginine (pH 7.4) at a flow rate of 0.5 ml/min. V_H elution was monitored via absorbance measurements at 280 nm.

Thioflavin T Fluorescence—Thioflavin T, a fluorescent dye that recognizes amyloid and some non-amyloid aggregates, was added to V_H samples (0.2 g/liter) to achieve a final thioflavin T concentration of 88 μM. Samples were excited at 450 nm, and emission was detected at 482 nm. The background buffer was also measured and its signal was subtracted from that of the samples. Samples were measured initially and after they had been heated to 95 °C and cooled to room temperature.

Antibody Binding Analysis—The binding of V_H domains was tested for multiple antigens. These antigens include Aβ42 fibril, freshly disaggregated Aβ42 (also referred to as Aβ monomer*), IAPP fibril, and freshly disaggregated IAPP (also referred to as IAPP monomer*). Disaggregated Aβ42 was generated by first incubating the lyophilized peptide (62-0-80, American Peptide) in hexafluoroisopropanol. Following overnight incubation, the hexafluoroisopropanol was removed by evaporation. The Aβ42 peptide was dissolved in 50 mM NaOH at a peptide concentration of 1 g/liter (220 μM), and then centrifuged at 208,000 RCF for 1 h at 4 °C. The top 80% of the supernatant was recovered and passed through a 0.22-μm filter (SLGV004SL, Millipore). The sample was then diluted into acidified PBS to achieve a final pH of 7.4 and a final peptide concentration of 25 μM. Aβ42 fibrils were formed by incubating disaggregated peptide at 37 °C without agitation for at least 2 days. Prior to using the Aβ42 fibrils for binding assays, they were sonicated on ice for 3 cycles of 10 s at 100% power with 30 s of rest between cycles (FB-120 Sonic Dismembrator, Thermo Fisher Scientific).

Disaggregated IAPP was prepared by dissolving the peptide in hexafluoroisopropanol. After lyophilization, the dried peptide was dissolved in 20 mM Tris (pH 7.4) to achieve a final concentration of 32 μM. IAPP fibrils were formed by incubating disaggregated IAPP at 37 °C (300 rpm) for at least 5 days. The IAPP fibrils were sonicated on ice for 10 s at 75% power (3 times) with 30 s of cooling between rounds of sonication.

The binding of V_H domains to Aβ and IAPP was characterized by an ELISA assay conducted in 96-well plates. The antigens were diluted to 2.5 μM, and 100 μl was added to a Nunc-Immuno 96-well plate with MaxiSorp surface coating (442404, Thermo Fisher Scientific) and incubated overnight at room

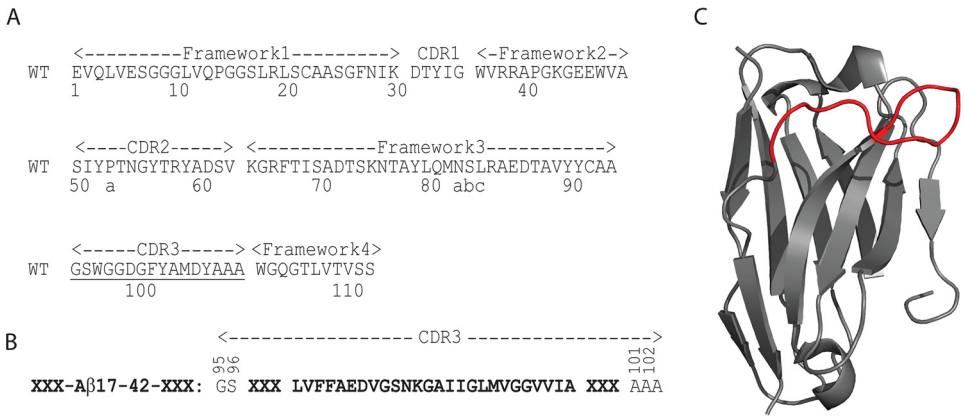

FIGURE 1. **Sequence of Aβ V_H domains and structure of the parent V_H domain.** *A*, amino acid sequence of the wild-type V_H domain, as defined using Kabat numbering. The C terminus also contained a 3× FLAG tag and a His_7 tag, whereas the N terminus contains residues Met-Ser-Lys-Leu (not shown). *B*, amino acid sequence of CDR3 for Aβ17–42 V_H domains. CDR3 positions flanking the grafted Aβ17–42 peptide (designated as *X*) were systematically varied with six identical residues that were charged (Asp, Glu, Arg, and Lys) or non-charged (Gln, Asn, Ser, Thr, and Ala). *C*, crystal structure of the parent wild-type V_H domain (Protein Data Bank 3B9V) with CDR3 highlighted in *red*.

temperature. Control wells without antigen were also included to determine the background signals. Milk dissolved in PBS (10% w/v) was then added to each well and incubated at room temperature for several hours before washing the wells with PBS. V_H domains that were labeled with a biotin tag (EZ-Link Sulfo-NHS-LC-Biotin, 21335, Thermo Fisher Scientific) were diluted to varying concentrations. At each concentration, 100 μl of the V_H domain sample was added to wells with immobilized antigen or background. The diluent for the V_H domains was 5% (w/v) milk in PBST supplemented with 0.02% (w/v) NaN_3 to reduce nonspecific interactions.

Following overnight incubation at room temperature, the biotinylated V_H domains were washed from the plate. HRP-conjugated streptavidin (21126, Pierce) was diluted 30,000-fold in PBST and 100 μl was added to the wells for incubation for 1 h at room temperature. The plate was washed a final time, and 100 μl of the substrate (1-Step Ultra TMB-ELISA Substrate Solution, 34028, Life Technologies) was added to each well. The plates were developed for 1–2 h and quenched with 2 M H_2SO_4 (100 μl). The absorbance signal at 450 nm was measured for each well using a Tecan Safire^2 plate reader. Signals were then normalized by subtracting the background value at each V_H concentration, and then dividing by the background. IC_{50} values were calculated from the resulting dose-response curve that was generated for each V_H domain.

The binding of V_H domains to different antigens was also characterized using an immunoblotting assay. The antigens (Aβ42 fibril and disaggregated Aβ42, IAPP fibril, and disaggregated IAPP) were immobilized on nitrocellulose membranes (10600004, GE Healthcare) by spotting 2 μl of each antigen at different concentrations. The membranes were then blocked in 10% (w/v) milk (dissolved in PBS) for 2 h at room temperature. After the blots were washed, solutions of biotinylated V_H domains (75 nM) in 5% (w/v) milk and PBST (supplemented with 0.02% w/v NaN_3) were added to the blots. After overnight incubation at room temperature with mild rocking, the blots were washed three times in PBST (10 min per wash). Next, HRP-conjugated streptavidin (21126, Pierce) was added that was diluted 45,000-fold in PBST, and the blots were incubated at room temperature for 1 h. The blots were then washed again with PBST (four times for 10 min per wash) before adding the substrate (Pierce ECL Western blotting Substrate, 32106, Thermo Fisher Scientific) and imaging the blots using an x-ray film developer (Konica Minolta SRX-101A).

Alanine Mutational Analysis of Aβ17–42 V_H Domain—Site-directed mutagenesis was used to generate variants of the V_H domain containing Aβ17–42 in CDR3 along with DDD at each edge of the grafted peptide. V_H domains were created in which three consecutive residues in CDR3 were replaced with three alanines. The variants examined were those in which residues in the linker region of the Aβ peptide (Aβ residues 22–29) were mutated to alanine.

Site-directed mutagenesis reactions were carried out using *PfuUltra* II Hotstart PCR Master Mix (600850, Agilent Technologies), which was added to a mixture of the template DNA, and forward and reverse primers. The PCR involved 19 cycles of denaturation at 95 °C for 30 s, followed by 1 min of annealing at 55 °C, and 12 min of extension at 68 °C. Following the PCR, the template DNA was digested by the addition of DpnI (R0176L, New England BioLabs Inc) for 2 h at 37 °C.

Results

Polar CDR3 Mutations Strongly Impact Expression Levels of Aβ V_H Domains—To examine the effect that different types of residues have on the solubility and conformational specificity of V_H domain antibodies grafted with a large amyloidogenic Aβ peptide (residues 17–42), we first cloned variants that contained the Aβ17–42 peptide flanked by three identical residues at each edge of CDR3 (Fig. 1). Variants studied included those with six identical residues that were negatively charged (DDD and EEE), positively charged (KKK and RRR), and non-charged (NNN, QQQ, SSS, TTT, and AAA).

After cloning the V_H domains, we expressed them in bacteria to evaluate how different CDR3 mutations affect their final yield after expression and purification. Our previous studies revealed that increased expression of Aβ V_H domains generally correlates with increased solubility (39, 40). Therefore, the relative amounts of expressed and purified V_H domains can potentially be used to evaluate their relative solubility. We found that the highest expressing Aβ17–42 V_H domains fol-

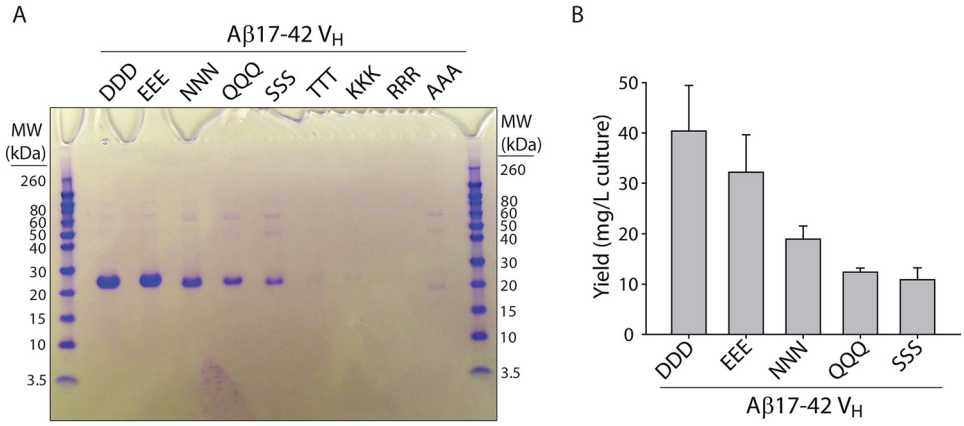

FIGURE 2. **Evaluation of the yield and homogeneity of purified Aβ17–42 V_H domains that were expressed in bacteria.** *A,* SDS-PAGE analysis of V_H domains purified using metal-affinity chromatography. The purified V_H domains were refolded, diluted 10-fold without normalizing their concentrations, analyzed using a 10% BisTris gel, and stained with Coomassie dye. *B,* yields of V_H domains after purification and refolding. The *error bars* are standard deviations for three replicates.

lowing purification and refolding were those with negatively charged mutations (DDD and EEE; Fig. 2).

In contrast, variants with positively charged residues (KKK and RRR) or small non-polar residues (AAA) expressed poorly (Fig. 2). SDS-PAGE analysis revealed that purified KKK and AAA V_H domains could only be detected using overloaded gels, whereas the RRR variant could not be detected (data not shown). Of the V_H domains with polar mutations, the TTT variant also expressed poorly (Fig. 2) and could only be detected via an overloaded SDS-PAGE gel (data not shown). Interestingly, V_H domains with NNN, QQQ, or SSS mutations in CDR3 were expressed at significant levels. Although the yields of these variants were lower than the DDD and EEE variants, the ability of these non-charged residues to promote expression of the hydrophobic Aβ17–42 V_H domain suggested that they increased antibody solubility.

The V_H domains were next refolded in 6 M GuHCl after purification. The recovery of the V_H domains after refolding was high (86–95%). Importantly, the refolding step resulted in improvements in the fraction of monomeric V_H domains, especially for the NNN, QQQ, and SSS variants (data not shown).

We next sought to evaluate whether the inability to express certain Aβ17–42 V_H domains was specific to our bacterial expression system or general to other expression hosts. This is a particularly important question for the KKK and RRR V_H domains because their low expression in bacteria may simply be due to their inability to translocate across the cytosolic membrane (46, 47) and not due to low solubility. Therefore, we also evaluated the expression levels of the V_H domains in *S. cerevisiae* (Fig. 3). To simplify the expression analysis, we cloned these domains as fusions to the C terminus of a yeast cell-surface protein (Aga2) and detected their display on the surface of yeast via a C-terminal myc tag.

Flow cytometry analysis revealed that the expression trends on the surface of yeast (Fig. 3) were similar to those observed for bacterial expression (Fig. 2). The expression levels of the negatively charged variants (DDD and EEE) as well as some of the non-charged variants (NNN, QQQ, and SSS) were higher than the other variants (KKK, RRR, TTT, and AAA; Fig. 3). Finally, we also evaluated expression of the KKK, AAA, and DDD variants as autonomous V_H domains in *P. pastoris* because this host is well known to produce recombinant proteins at high levels. However, we found that expression of only the DDD variant could be detected (data not shown). These findings collectively suggest that negatively charged and some non-charged residues (asparagine, glutamine, and serine) are best at promoting expression of the hydrophobic Aβ17–42 V_H domain.

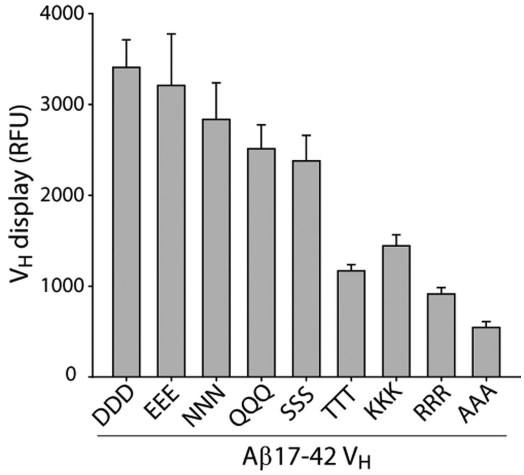

FIGURE 3. **Evaluation of yeast surface display levels of Aβ17–42 V_H domains.** The V_H domains were fused to the C terminus of an *S. cerevisiae* cell-surface protein (Aga2), and the level of surface display was evaluated by flow cytometry via antibody binding to a myc tag at the C terminus of the Aga2-V_H fusions. The data are averages of five independent experiments, and the *error bars* are standard deviations.

Non-charged Polar CDR3 Mutations Promote High Conformational Stability of V_H Domains—We next sought to evaluate the secondary structures and stabilities of the Aβ17–42 V_H domains with negatively charged (DDD and EEE) or non-charged (NNN, QQQ, and SSS) residues. We reasoned that the conformational stability of the non-charged polar variants may be higher due to the potentially unfavorable impact of the negatively charged residues on the stability of the grafted V_H domains. Circular dichroism analysis revealed that the secondary structures of the charged and uncharged variants were typical of β-sheet-rich V_H domains (data not shown).

To evaluate the potential impact of negatively charged mutations relative to non-charged ones on V_H conformational sta-

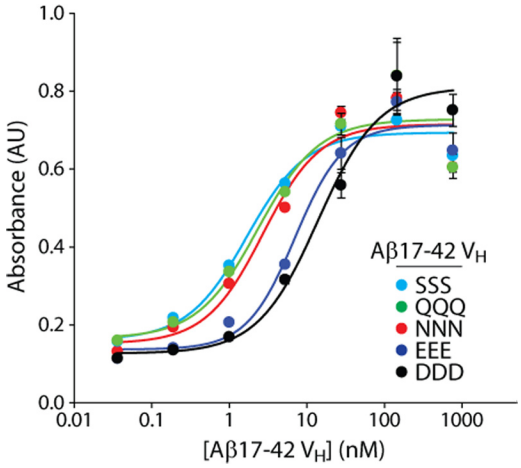

FIGURE 4. **Effect of mutations at the edges of CDR3 on the binding of Aβ17–42 V_H domains to a conformational ligand (Protein A).** Protein A was immobilized in well plates, V_H domains were added at a range of concentrations, and their relative binding was evaluated. The Aβ17–42 V_H domain is a V_H3 domain and has a Protein A binding site on its framework. The *error bars* are standard deviations for two replicates.

TABLE 1

Apparent folding stabilities and relative Protein A affinities for Aβ17–42 V_H domains with three identical polar residues inserted at each edge of CDR3

Aβ17–42 V_H	Protein A IC_{50}[a]	T_m
	nM	℃
DDD	10.1 ± 0.4	68.7 ± 0.4[b]
EEE	5.2 ± 1.1	71.4 ± 0.5[b]
NNN	1.9 ± 0.2	75.4 ± 0.6[c]
QQQ	2.1 ± 1.0	75.8 ± 0.6[c]
SSS	1.3 ± 0.2	75.0 ± 0.7[c]

[a] Experiments were run in duplicate, and the averages and standard deviations are reported.
[b] T_m values were calculated from the first melt.
[c] Apparent T_m values were calculated from the first melt.

bility, we first analyzed the relative affinity of the Aβ17–42 domains for Protein A. This analysis is motivated by the fact that folded V_H3 domains (such as the Aβ17–42 domains) have a Protein A binding site on their scaffold, and the relative binding of Protein A to V_H3 domains is correlated with V_H stability (45, 48, 49). Using an ELISA assay to measure V_H binding to immobilized Protein A, we found that the NNN, QQQ, and SSS variants had similar IC_{50} values of ~1–2 nM, whereas the DDD and EEE variants had higher IC_{50} values (~5–10 nM; Fig. 4 and Table 1). The higher IC_{50} values for the negatively charged variants suggested they are less stable than the other polar variants, which may be due to intramolecular repulsion.

We further examined the conformational stability of the Aβ17–42 V_H domains by measuring their apparent melting temperature (T_m) values using circular dichroism. The DDD and EEE variants had lower T_m values (~69 and ~71 °C, respectively) than the NNN, QQQ, and SSS variants (~75 °C; Fig. 5 and Table 1). These findings are consistent with the Protein A results (Fig. 4) and also suggest that the V_H domains with negatively charged mutations in CDR3 are less conformationally stable than the variants with non-charged mutations.

Aspartate, Glutamate, and Asparagine Increase Solubility and Prevent Irreversible Unfolding of V_H Domains—We have previously found that negatively charged mutations in CDR3 of grafted V_H domains prevent irreversible unfolding of some hydrophobic V_H domains but not others (39, 40). Thus, we sought to evaluate if the DDD and EEE variants promoted reversible unfolding and refolding of the Aβ17–42 V_H domains as well as to what extent non-charged mutations could promote such reversible unfolding. Circular dichroism was used to monitor the ellipticity of the samples at a fixed wavelength (235 nm) as a function of temperature. The DDD and EEE variants showed largely reversible unfolding and refolding behavior (Fig. 5), consistent with our previous findings (39, 40, 50). Surprisingly, the NNN variant also displayed unfolding behavior that was largely reversible, whereas the QQQ and SSS variants unfolded irreversibly. These differences were also apparent in terms of the circular dichroism spectra at 25 °C for V_H domains before and after being heating to 95 °C. The DDD, EEE, and NNN V_H variants largely regained their initial secondary structure after being heated to 95 °C and cooled, whereas the secondary structure of the QQQ and SSS variants was significantly perturbed (data not shown).

These results suggested that the QQQ and SSS V_H domains aggregated at high temperature. To investigate this in more detail, we performed solubility measurements after heating the Aβ17–42 V_H domains to different temperatures (50–95 °C) and cooling them to 25 °C (Fig. 6). The solubility of the DDD and EEE variants was high and unaffected by heat stress (Fig. 6*A*). The NNN V_H variant was modestly less soluble than the DDD and EEE variants, but significantly more soluble than the QQQ and SSS variants. These solubility differences appear related to the formation of amyloid-like aggregates (Fig. 6*B*). The QQQ and SSS V_H domains displayed high thioflavin T fluorescence after heating, whereas the other polar variants displayed similar (DDD) or modestly increased (EEE and NNN) thioflavin T fluorescence after heating.

We also investigated the relative solubility of the Aβ17–42 V_H domains at room temperature (25 °C) and a higher antibody concentration (~50 μM) over the course of a week (Fig. 7) to evaluate similarities or differences with the non-native solubility data (Fig. 6). Samples were evaluated for their fractional monomer content using size exclusion chromatography. The monomer content of the DDD and EEE variants remained constant at ~90% over the course of 1 week at 25 °C. The NNN variant had a lower initial monomer content (~65%), which remained roughly constant after 1 week. The other variants that initially contained 66% (QQQ) and 53% (SSS) monomer displayed further aggregation over the course of 1 week. These findings reveal that the relative native and non-native solubilities of the Aβ17–42 domains display similar trends, which is consistent with our hypothesis that the solvent-exposed Aβ17–42 peptide in CDR3 mediates aggregation of both unfolded and folded V_H domains.

To evaluate the generality of our findings, we also sought to design a grafted V_H domain specific for IAPP. IAPP is extremely amyloidogenic and several small peptide segments derived from residues 8–37 are known to form fibrils (51–55). Thus, we chose to graft this large peptide segment (residues 8–37) into CDR3 along with negatively charged residues (DED) at each edge of CDR3. This IAPP8–37 V_H domain expressed well (94 mg/liter) and showed similar secondary structure as the DDD

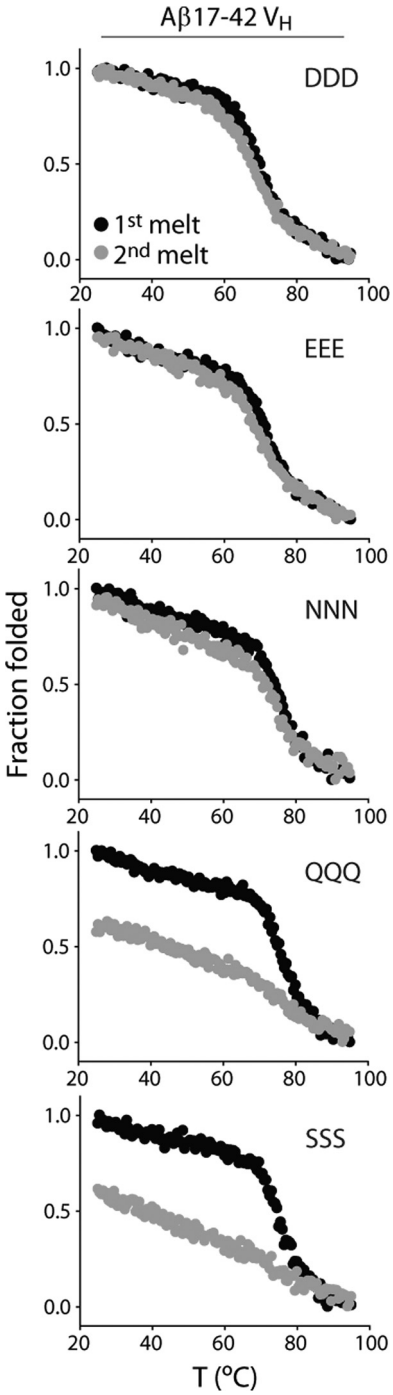

FIGURE 5. **Impact of mutations at the edges of CDR3 on the apparent folding stability and reversibility of unfolding of the Aβ17–42 V_H domains.** The ellipticity signal at 235 nm was monitored as a function of temperature using circular dichroism. Each V_H domain was cooled to 25 °C after its initial melt, and then melted a second time to evaluate reversibility.

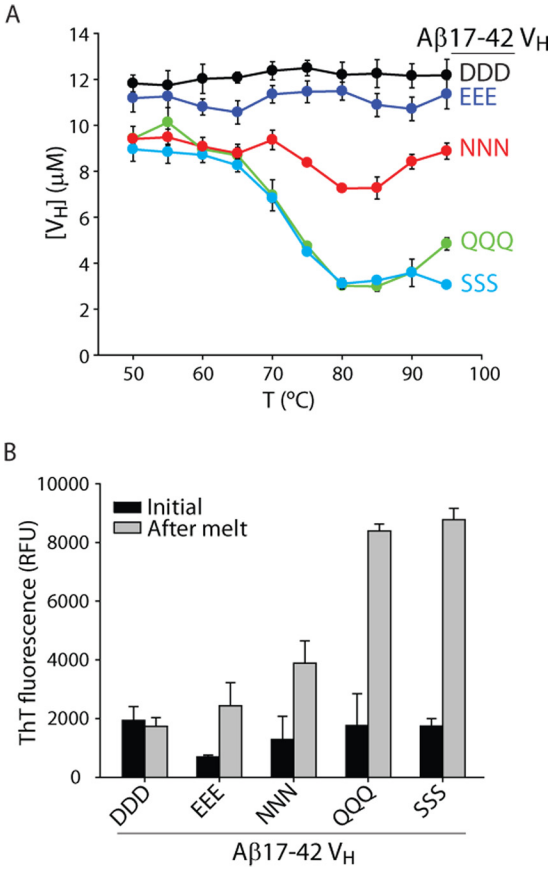

FIGURE 6. **Characterization of the relative solubility of Aβ17–42 V_H domains after heat stress.** *A,* the concentration of soluble V_H domain after heating for 20 min, cooling to room temperature, and sedimenting insoluble antibody. *B,* thioflavin T (*ThT*) fluorescence for V_H domains at room temperature before and after being heating to 95 °C. In *A*, the *error bars* are standard deviations for three replicates. In *B*, the *error bars* are standard deviations for two replicates.

Aβ17–42 V_H domain (data not shown). Upon thermal denaturation, it was also able to unfold in a nearly reversible manner (Fig. 8*A*), its melting temperature (71 °C) was similar to those of the DDD and EEE Aβ17–42 V_H domains (69–71 °C), and it was largely monomeric like the DDD Aβ17–42 V_H domain (Fig. 8*B*). In contrast, the same IAPP8–37 V_H domain with NNN residues at each edge of CDR3 showed reduced expression (15 mg/liter), suggesting that the negatively charged residues enhanced solubility of this antibody domain.

Charged and Non-charged Polar Mutations Differentially Impact the Conformational Specificity of Aβ V_H Domains—The significant effect of the polar mutations flanking the Aβ17–42-grafted peptide on V_H solubility led us to also evaluate how such mutations influence antigen binding. Using an ELISA assay to measure concentration-dependent binding, we found that the DDD, NNN, QQQ, and SSS variants all recognized Aβ42 fibrils. The EEE variant was not evaluated in detail because it displays similar binding activity as the DDD variant (data not shown). The fibril IC_{50} values were lowest for the DDD (43 ± 15 nM) and NNN (43 ± 12 nM) variants, and highest for the QQQ (114 ± 75 nM) and SSS (346 ± 64 nM) variants (Fig. 9*A* and Table 2). Interestingly, the most significant difference between the Aβ17–42 V_H domains was their ability to recognize disaggregated Aβ. The negatively charged (DDD) variant showed little binding to disaggregated Aβ42 (Fig. 9*A*). In contrast, V_H variants with non-charged mutations were able to bind to disaggregated Aβ42. The SSS and QQQ variants displayed increased binding signals for disaggregated Aβ relative to fibrils. The IC_{50} values for binding of the NNN, QQQ, and SSS variants to disaggregated Aβ were similar (200–300 nM; Table 2).

Given that some of the V_H domains form higher order species (Fig. 7*A*), we evaluated whether such multimers may influence the observed conformational specificity or IC_{50} values of

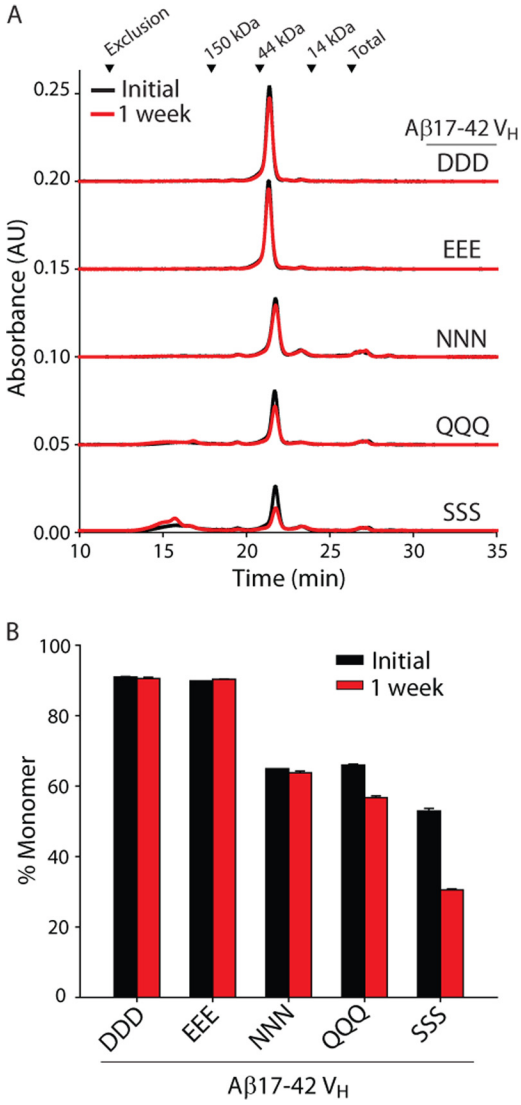

FIGURE 7. **Size exclusion chromatography analysis of the Aβ17–42 V_H domains.** *A,* V_H domains were analyzed after refolding (initial) and 1 week of incubation at 25 °C after refolding. *B,* the fraction of monomer for the Aβ17–42 V_H samples, as judged by the chromatograms in *A*.

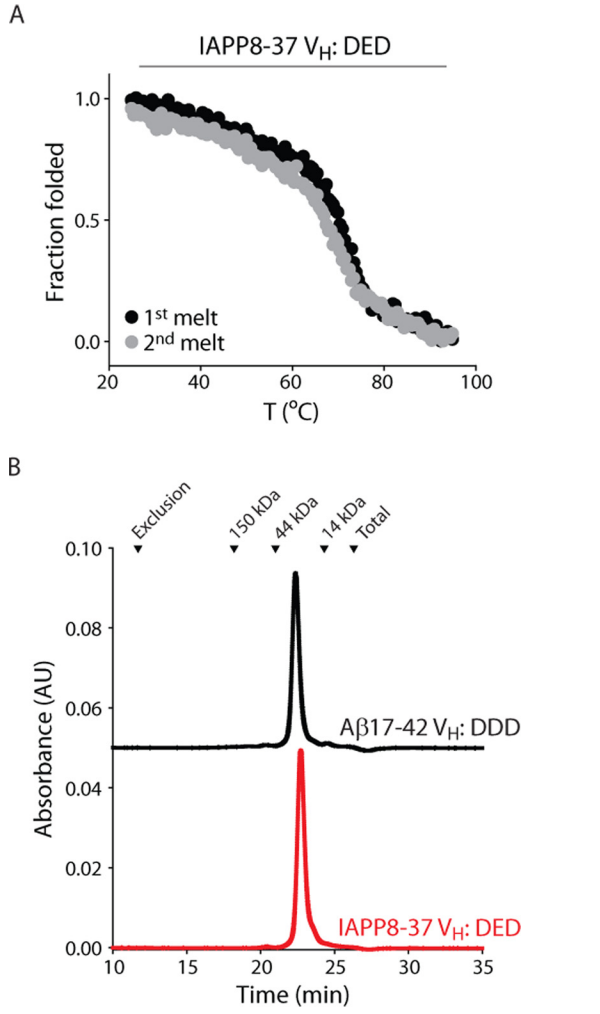

FIGURE 8. **Biophysical properties of the IAPP8–37 V_H domain with negatively charged residues (DED) at the edges of CDR3.** *A,* evaluation of the apparent folding stability and reversibility of unfolding of the IAPP8–37 V_H domain. The ellipticity signal of the V_H domain was monitored at 235 nm using circular dichroism. *B,* size exclusion chromatograms for the IAPP8–37 (DED) and Aβ17–42 (DDD) V_H domains. The chromatograms are shifted vertically for clarity. The CDR3 sequence of the IAPP8–37 V_H domain was DED-ATQRLANFLVHSSNNFGAILSSTNVGSNTY-DED. The sequence of the rest of the IAPP8–37 V_H domain (including the edges of CDR3) is the same as in Fig. 1 for the Aβ17–42 V_H domains.

the Aβ17–42 V_H domains. To accomplish this, we enriched the fraction of V_H monomer in the purified samples for the QQQ and SSS V_H domains and evaluated their binding. A rigorous centrifugation step (208,000 RCF for 1 h) reduced the fraction of high molecular weight species from 15 ± 1 to 9 ± 1% for the QQQ V_H domain and from 17 ± 1 to 11 ± 1% for the SSS V_H domain.

For the QQQ and SSS V_H domains, samples with reduced aggregate content had IC_{50} values that were within error of the control samples for binding to disaggregated Aβ (data not shown). This suggests that the presence of V_H multimers did not significantly affect binding. Interestingly, we observed that the reduction of V_H multimers modestly enhanced the normalized binding signals (data not shown). Collectively these findings suggest that the enhanced binding of the QQQ and SSS V_H domains (relative to the DDD variant) to disaggregated Aβ is not strongly linked their higher aggregate content.

We also found that the polar residues at the edges of CDR3 influenced the sequence specificity of the Aβ17–42 V_H domains. The DDD variant displayed high specificity for Aβ fibrils relative to IAPP fibrils (Fig. 9*A*). The NNN, QQQ, and SSS variants bound preferentially to Aβ fibrils but also displayed modest binding to IAPP fibrils. We confirmed that the specificity of the Aβ17–42 V_H domains for Aβ fibrils was not simply due to low reactivity of IAPP fibrils by evaluating binding of the IAPP8–37 V_H domain (Fig. 9*B*). This V_H domain with DED residues at the edges of CDR3 recognized IAPP fibrils (IC_{50} value of 126 ± 68 nM) and weakly bound to either Aβ conformer.

We also evaluated the binding activity of the Aβ and IAPP V_H domains using an immunoblotting assay (Fig. 10). Aβ42 and IAPP fibrils and disaggregated peptides were deposited on nitrocellulose membranes at a range of concentrations and probed with V_H domains as well as with conventional antibodies. The DDD Aβ17–42 V_H domain displayed significant conformational specify for Aβ fibrils relative to disaggregated Aβ

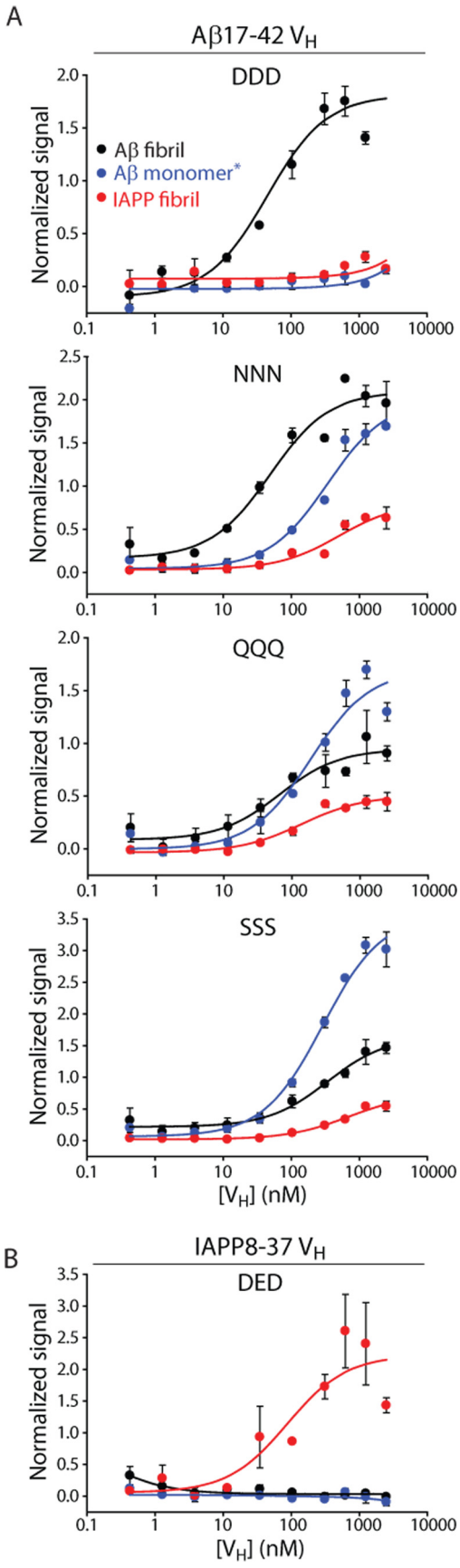

FIGURE 9. **Impact of mutations at the edges of CDR3 on the conformational specificity of the Aβ17–42 and IAPP8–37 V_H domains.** *A*, binding of Aβ17–42 V_H domains to immobilized Aβ42 fibrils and disaggregated Aβ42 (referred to as monomers*) relative to IAPP fibrils. *B*, binding of the IAPP8–37 V_H domain (defined in Fig. 8) to IAPP fibrils relative to Aβ42 fibrils and monomers*. The normalized binding values are reported as signal minus background divided by background. For each experiment, two replicates were collected for each point, and the standard deviations are reported. The experiments were performed at least three times for each V_H domain, and data from one representative experiment is shown.

TABLE 2
Aβ conformational specificity for Aβ17–42 V_H domains with three identical polar residues inserted at each edge of CDR3
Freshly disaggregated Aβ42 is referred to as monomer*.

Aβ17–42 V_H	IC_{50}	
	Aβ42 fibril	Aβ42 monomer*
	nM	*nM*
DDD	43 ± 15	ND
NNN	43 ± 12	251 ± 87
QQQ	114 ± 75	281 ± 105
SSS	346 ± 64	297 ± 75

[a] ND, not determined

and little cross-reactivity with IAPP conformers. The NNN, QQQ, and SSS variants displayed similar binding to fibrils. However, they also weakly recognized disaggregated Aβ (Fig. 10), which is generally consistent with the ELISA results (Fig. 9). Moreover, the background signals for the NNN V_H domain and especially for the QQQ and SSS V_H domains were higher than for the DDD variant. This suggests that the non-charged variants were stickier and less well suited for immunoblotting applications. Interestingly, the specificity of conventional antibodies (LOC and OC) with conformational specificity for Aβ fibrils was only observed at the lowest amounts of deposited Aβ (0.5 pmol). Moreover, these antibodies that recognize fibrils of different amyloid-forming polypeptides (19, 56, 57) either failed to recognize IAPP fibrils or recognized both IAPP conformers after long exposure times (LOC, data not shown). As expected, conventional antibodies that recognize sequence-specific epitopes within Aβ42 (NAB 228, 12F4, and 4G8) recognized both Aβ fibrils and disaggregated Aβ.

Conversely, we observed that the IAPP8–37 V_H domain selectively recognized IAPP fibrils relative to disaggregated IAPP, and showed low cross-reactivity with Aβ conformers (Fig. 10). This is in contrast to a conventional IAPP sequence-specific antibody (R10/99) that recognized both IAPP conformers. These results collectively demonstrate that V_H domains grafted with amyloidogenic peptides can be generated with sequence and conformational specificity for amyloid fibrils.

Conformational Specificity of the DDD Aβ17-42 V_H Appears to be Mediated by Repulsive Electrostatic Interactions—The fact that the DDD variant of the Aβ17–42 V_H weakly recognizes disaggregated Aβ relative to the other Aβ V_H variants without charged mutations suggests that repulsive electrostatic interactions may mediate the conformational specificity of the DDD variant. This is further supported by the fact that Aβ42 is predicted to have an acidic isoelectric point (~5) and contains six negatively charged residues, some of which are adjacent to the most amyloidogenic regions. To test this hypothesis, we compared the binding of the DDD Aβ17–42 V_H to Aβ and IAPP conformers at normal (0.14 M) and elevated (1 M) concentrations of sodium chloride (Fig. 11*A*). Importantly, this V_H domain displayed significantly enhanced binding to disaggre-

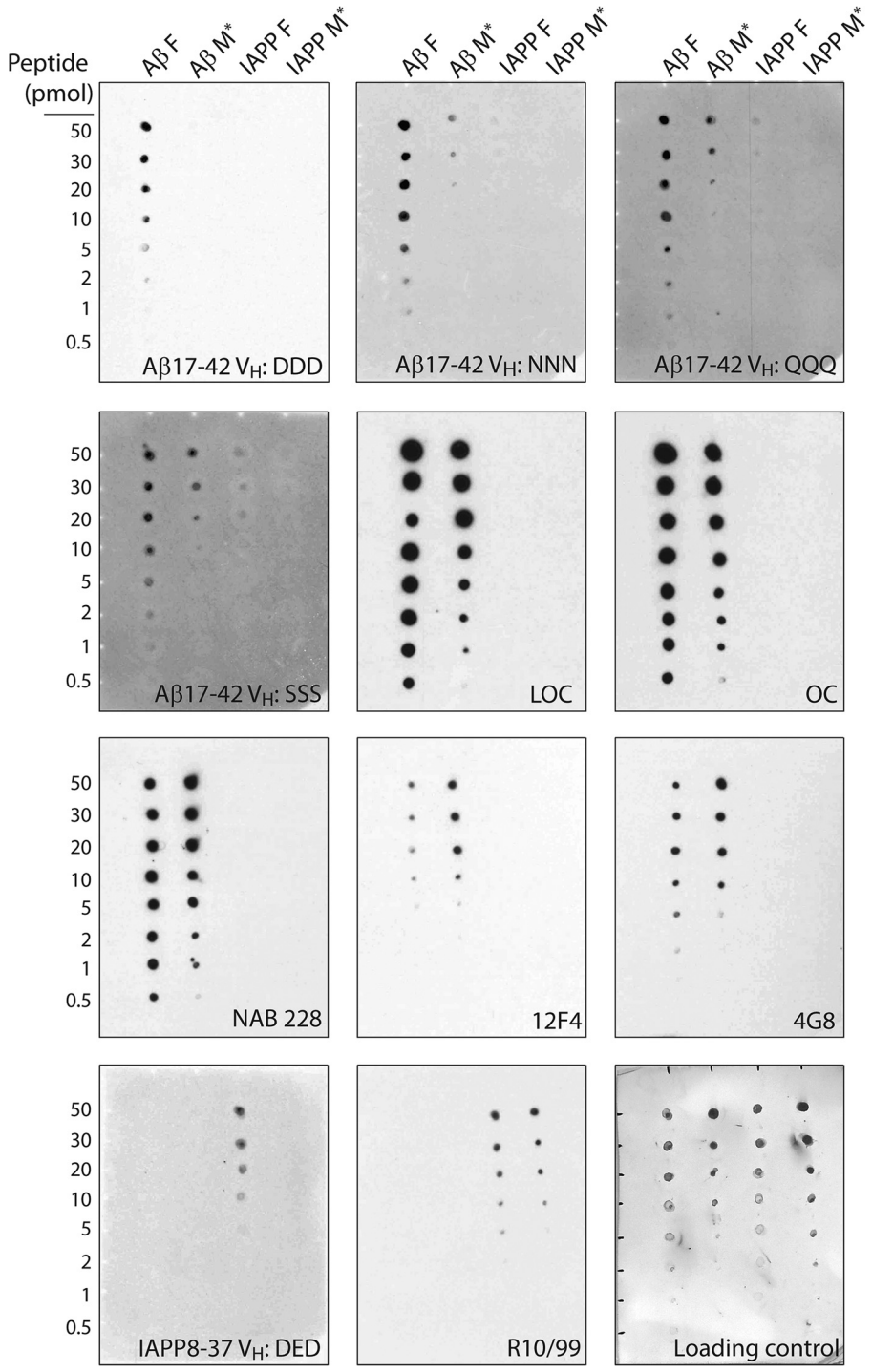

FIGURE 10. **Evaluation of the conformational and sequence specificity of the Aβ17–42 and IAPP8–37 V_H domains relative to conventional antibodies using an immunoblotting assay.** Aβ42 and IAPP fibrils (*F*) and freshly disaggregated peptide (referred to as monomers*, *M*) were deposited at various concentrations on nitrocellulose membranes. The binding of Aβ17–42 V_H domains (75 nM) was evaluated for variants with negatively charged (DDD) or non-charged (NNN, QQQ, and SSS) residues at each edge of the grafted amyloid peptide. An IAPP8–37 V_H domain (75 nM) with DED residues at each edge of CDR3 was also tested. Their behavior was compared with that of conventional antibodies with conformational specificity (LOC and OC; ×2500 dilution) or sequence specificity for Aβ (NAB 228, 12F4, and 4G8; ×500–2000 dilution) or IAPP (R10/99; ×100 dilution). A loading control blot was developed using silver colloidal stain.

gated Aβ at high salt, and did not show increased binding to IAPP conformers. The DDD Aβ17–42 V_H also displayed modest increases in its binding signals for Aβ fibrils.

We also evaluated whether the enhanced binding of the DDD antibody variant to Aβ at high salt was mediated by salt-induced V_H oligomerization. To test this possibility, we used size exclusion chromatography to analyze the potential oligomerization of the DDD Aβ17–42 V_H as a function of salt concentration. However, the levels of the high molecular weight species of the DDD V_H domain were a weak function of salt (5% at 0.14 M NaCl, 6% at 1 M NaCl). Thus, we conclude that the enhanced affinity of the Aβ17–42 V_H for disaggregated Aβ is

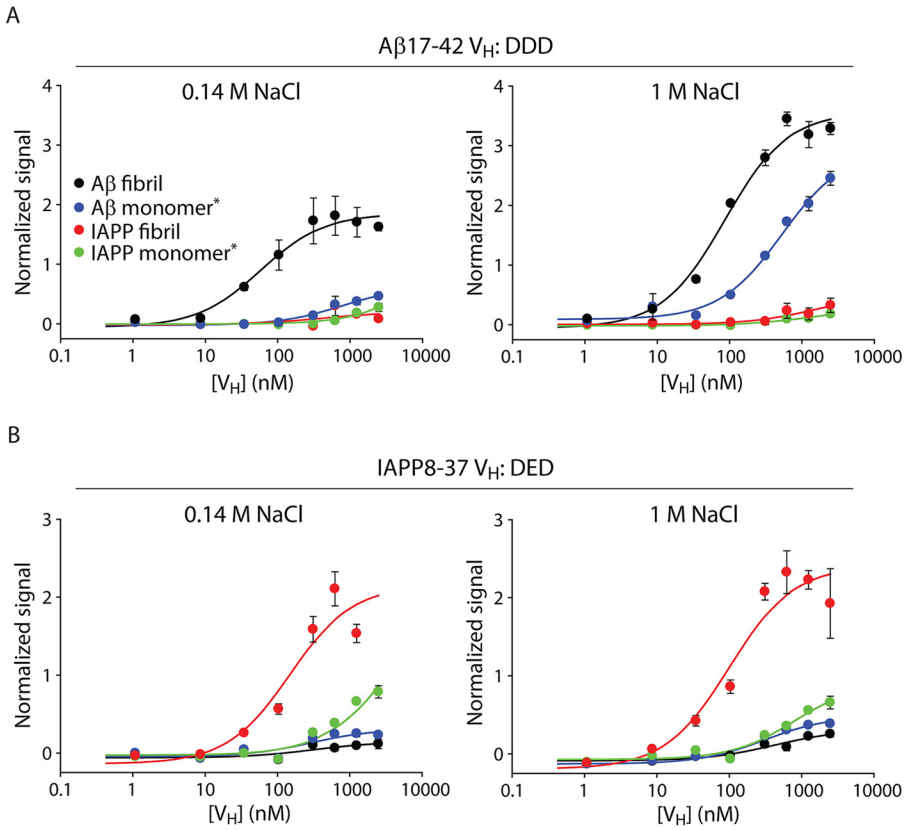

FIGURE 11. **Impact of salt concentration on the conformational specificity of the Aβ17–42 and IAPP8–37 V_H domains.** Aβ42 and IAPP fibrils and freshly disaggregated peptide (referred to as monomers*) were immobilized in well plates, and the binding of Aβ17–42 (*A*) and IAPP8–37 (*B*) V_H domains was evaluated at low (0.14 M) and high (1 M) NaCl concentrations at pH 7.4 (10 mM phosphate). The V_H domains contained negatively charged residues at each edge of CDR3 (DDD for Aβ17–42, DED for IAPP8–37). The normalized binding values are reported as signal minus background divided by background. Two replicates were collected for each point, and the standard deviations are reported. The experiments were performed at least three times for each V_H domain, and data from one representative experiment is shown.

likely due to the screening of repulsive electrostatic interactions rather than salt-induced oligomerization of the V_H domain.

The enhanced binding for the DDD Aβ17–42 V_H to Aβ42 monomer (pI ~5) at high salt suggests that repulsive electrostatic interactions influence the corresponding conformational specificity. In contrast, IAPP is a basic polypeptide (theoretical pI of >10) with only three residues that potentially could be charged (Lys^1, Arg^{11}, and His^{18}) and which are peripheral to the most amyloidogenic region (IAPP residues 22–27). Thus, we expected that the binding of the IAPP8–37 V_H with negatively charged residues (DED) at the edges of CDR3 would be weakly impacted by changes in salt concentration. Indeed, we find that high salt does not alter IAPP8–37 V_H binding to IAPP or Aβ conformers (Fig. 11*B*). These results reveal important differences in the mechanisms of conformational specificity for the Aβ and IAPP V_H domains.

Alanine Mutational Analysis Reveals That Aβ Residues 22–29 Modulate Expression and Binding of the DDD Aβ17-42 V_H—We next generated and analyzed a series of alanine mutations in CDR3 of the DDD Aβ17–42 V_H to understand how residues within the grafted Aβ peptide modulate antibody expression and binding. We focused on Aβ residues ^{22}EDVGSNKG^{29} that link the two major aggregation-prone regions (Aβ residues ^{17}LVFFA^{21} and ^{31}IIGLMVGGVVIA^{42}) within Aβ42. Mutants were generated in which three consecutive residues were replaced by three alanines.

We find that Aβ residues ^{21}AED^{23} are critical for expression, as mutating them to alanines significantly reduced V_H expression (Fig. 12*A*). Likewise, mutation of residues ^{27}NKG^{29} to three alanines greatly reduced expression. However, mutation of Aβ residues ^{23}DVG^{25} or ^{25}GSN^{27} to three alanines resulted in Aβ17–42 V_H domains with similar or modestly lower expression levels relative to wild-type V_H (Fig. 12*A*). Size exclusion chromatograms and far-UV CD spectra for the mutants and wild-type were also similar (data not shown). Their binding behavior, however, was significantly different (Fig. 12*B*). The ^{23}AAA^{25} and ^{25}AAA^{27} V_H mutants bound to disaggregated Aβ better than wild-type. These findings indicate that hydrophilic Aβ residues 22–29 generally reduce Aβ self-association and increase solubility, and that Aβ residues 23–27 reduce Aβ17–42 V_H binding to disaggregated Aβ.

Discussion

Our studies aimed at designing anti-amyloid antibody fragments were originally motivated by a previous report using a similar motif-grafting approach to generate full-length antibodies specific for aggregated forms of the mammalian prion protein (PrP) (58). These antibodies were generated by grafting PrP peptides containing residues 89–112 (24-mer) or 136–158 (23-mer) into heavy chain CDR3 of an antibody originally specific for an HIV protein. These peptides were identified based on their importance in mediating conversion from PrP^C to

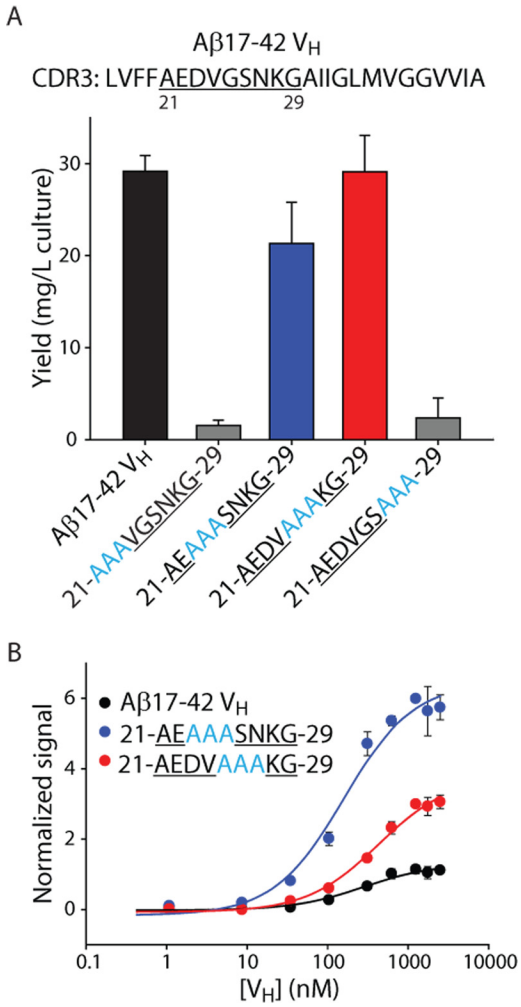

FIGURE 12. **Effect of alanine substitution mutations in CDR3 on expression and binding for the Aβ17–42 V_H domain.** Three consecutive residues in the grafted Aβ17–42 peptide were replaced with three alanines. *A*, yields of V_H domains after purification and refolding. *B*, binding of V_H domains to immobilized, disaggregated Aβ peptide. The V_H domains contained three negatively charged residues (DDD) at each edge of the grafted Aβ17–42 peptide in CDR3. In *A*, the averages and standard deviations for two replicates are shown. In *B*, each point is the average of two replicates, the experiments were performed twice, and data from one representative experiment is shown.

PrP^{Sc} (29, 59–63). The resulting grafted antibodies recognized the aggregated, infectious form of PrP (PrP^{Sc}) but not the soluble, non-infectious form (PrP^{C}).

Notably, the grafted PrP peptides each contain four positively charged residues (58, 64). Mutating these residues to alanine eliminates binding for the grafted variant with PrP residues 89–112 in heavy chain CDR3 (this analysis was not reported for the other variant). A third PrP peptide (residues 19–33) was later identified that also mediates binding to aggregated forms of PrP when grafted into heavy chain CDR3 (64). This peptide also contains four positively charged residues and binding is eliminated when such residues are mutated to alanine. Collectively these results suggest that the binding mechanism of these PrP conformational antibodies involves electrostatic interactions.

Our results suggest that Aβ and IAPP-grafted antibody domains employ non-electrostatic interactions to mediate binding to amyloid aggregates. This is supported by the fact that fibril binding for the Aβ17–42 and IAPP8–37 V_H domains with negatively charged CDR3 mutations is similar or better at high salt than at low salt (Fig. 11). Moreover, fibril binding for Aβ17–42 V_H domains was similar for CDR3 mutations that have side chains of similar size (aspartate and asparagine; Fig. 9).

Nevertheless, we find that repulsive electrostatic interactions are important for determining the affinity of Aβ17–42 V_H binding to disaggregated Aβ. Addition of negatively charged residues (DDD) at the edges of the grafted Aβ17–42 peptide reduced V_H binding to disaggregated Aβ, whereas removal of negative charge in the grafted Aβ17–42 peptide (^{23}DVG^{25} to ^{23}AAA^{25}) increased V_H binding. These findings suggest that the conformational specificity of the Aβ17–42 V_H for binding to Aβ fibrils relative to disaggregated Aβ is strongly mediated by repulsive electrostatic interactions.

Collectively our results suggest that the mechanism for the conformational specificity of the DDD Aβ17–42 V_H domain is due to multiple contributions. One factor may be the entropic penalty for binding of the grafted Aβ17–42 peptide to disaggregated Aβ, the latter of which is largely unstructured. We reason that the interaction of this grafted V_H domain with Aβ fibrils is more favorable because of the lower entropic penalty for binding to structured fibrils. A second factor that appears to contribute to the conformational specificity of the DDD Aβ17–42 V_H domain is electrostatic repulsion between negatively charged residues in CDR3 and those within Aβ. We speculate that the DDD variant binds to Aβ fibrils because amyloidogenic (homotypic) interactions involving Aβ residues 17–42 are more significant than the repulsive electrostatic interactions that discourage binding to disaggregated Aβ. It is also possible that the effective net charge of Aβ within structured fibrils is lower than for disaggregated Aβ, which may also contribute to the observed conformational specificity. Moreover, avidity effects due to the polyvalent nature of aggregates relative to monomers may also contribute to the observed conformational specificity (65).

Our findings for the DED IAPP8–37 V_H domain provide further insight into the mechanisms of conformational specificity for such grafted antibodies. Notably, this V_H domain binds well to IAPP fibrils and poorly to disaggregated IAPP. The fact that the IAPP peptide contains little charge and that the conformational specificity of the DED IAPP8–37 V_H domain is insensitive to salt concentration suggests that its binding mechanism is largely mediated by non-electrostatic interactions. The conformational specificity of this V_H domain may be due to the reduced entropic penalty for binding to structured fibrils relative to disordered peptide and/or avidity effects due to polyvalent aggregates. These speculative conclusions will need to be tested for additional grafted V_H domains and using different types of aggregates.

The fact that the expression levels of the Aβ17–42 V_H domains were strongly influenced by elimination of charged residues in the grafted Aβ17–42 peptide also deserves further consideration. Our alanine mutational data revealed that Aβ residues ^{22}ED^{23} are critical for expression, which is consistent with previous studies that have highlighted the importance of these residues for Aβ solubility (66–68). Deletion or substitu-

tion of these negatively charged residues for non-charged or positively charged residues, as occurs for Aβ variants associated with familial forms of Alzheimer disease, has been found in some cases to significantly increase the aggregation rates of Aβ (69–71).

Our findings related to the impact of CDR3 mutations on V_H solubility also deserve further consideration. We have previously shown that negatively charged mutations are effective at increasing the solubility of V_H domains grafted with shorter (10-mer) amyloidogenic peptides (39, 40), which is consistent with our findings here. Moreover, we have also previously found that positively charged mutations are less effective at increasing expression and solubility of grafted V_H domains unless the antibody scaffold has a highly basic isoelectric point (39). Our current findings for a scaffold with a near-neutral isoelectric point (theoretical pI of ~8.5 when omitting the CDRs and FLAG tags) are consistent with our previous observations given the low expression levels of the Aβ17–42 V_H domains with positively charged mutations in both *Escherichia coli* and *P. pastoris*, as well as the low display levels of such variants on the surface of *S. cerevisiae*.

It is notable that the polar residues asparagine, glutamine, and serine enabled V_H expression at sufficient levels for purification and analysis, whereas threonine did not. Moreover, asparagine was found to be most solubilizing, followed by glutamine and serine. We originally posited that serine would be the most solubilizing of these polar residues for multiple reasons. First, we suspected that the propensity of polyglutamine and polyasparagine to self-associate and aggregate (72, 73) would make these residues less solubilizing than multiple serines when introduced into CDR3. Moreover, previous work by others demonstrated that serine is the most solubilizing non-charged residue when introduced into a solvent-exposed loop within Ribonuclease Sa (74). However, there are several key differences between this previous study and our study, including the number of mutations (one for Ribonuclease Sa and six for V_H domains) and the solution conditions (1–2 M ammonium sulfate at pH 4.25 for Ribonuclease Sa and PBS at pH 7.4 for our V_H domains) that make it difficult to compare them.

Nevertheless, our findings are consistent with several hydropathy indices that report asparagine as the most hydrophilic non-charged residue followed by glutamine, serine, and threonine (in that order) (75, 76). Thus, it is possible that residues such as asparagine and glutamine are simply increasing the local hydrophilicity adjacent to the grafted hydrophobic peptides and thereby increasing V_H solubility. Moreover, it is likely that six asparagine or glutamine residues in CDR3 are unable to mediate the aggregation observed for longer repeat lengths of polyasparagine and polyglutamine (73, 77). It is also notable that hydropathy indices do not describe the overall solubility trends we observed for charged and non-charged residues. In particular, positively charged mutations are typically predicted to be more hydrophilic than non-charged polar residues and, in some cases, more hydrophilic than negatively charged residues (75, 76).

We have also identified a number of factors that influence the performance of our grafted V_H domains. First, we find that the longer grafted Aβ (26-mer) and IAPP (30-mer) peptides lead to improved binding relative to the shorter (10-mer) grafted peptides that we have previously reported (38–40, 78). Our findings as well as those for PrP antibodies (58, 64) suggest that peptide lengths of 23–30 residues are a logical starting point for designing antibodies and antibody fragments specific for other amyloid-forming polypeptides. Second, we find that our V_H domains display some propensity to interact non-specifically with well plates and immunoblotting membranes unless the experiments are performed in milk. Thus, it is important to block well plates and membranes with 10% milk, and conduct the binding experiments in at least 5% milk using our V_H domains. This also suggests that the Aβ and IAPP V_H domains are not appropriate for use in assay formats that are incompatible with milk.

We also find that the detection sensitivity is higher using biotin-based detection (streptavidin-HRP) than peptide tag-based detection (anti-FLAG and secondary antibody-HRP). Thus, it is recommended to biotinylate the V_H domains at low levels (~4–7 biotins per domain) to maximize specificity and detect them using standard biotin-specific reagents. Moreover, we find that sequence specificity of the V_H domains is reduced as the amount of immobilized antigen is increased in immunoblotting assays. For the NNN, QQQ, and SSS Aβ17–42 V_H domains, we observe some cross-reactivity with IAPP fibril in well plates at V_H concentrations >100 nM (Fig. 9). We also sometimes observe cross-reactivity of the Aβ17–42 (DDD) and IAPP8–37 (DED) V_H domains with non-cognate antigens such as α-synuclein and Tau for immunoblots loaded with >200 ng of protein (data not shown). Thus, it is important to evaluate the binding of such V_H domains over a range of amounts of immobilized antigen to identify suitable conditions for maximizing sequence specificity.

We also find that the assay format influences the extent of conformational specificity of the V_H domains. The Aβ17–42 (DDD) and IAPP8–37 (DED) V_H domains show significant conformational specificity both in well plates and immunoblot assays (Figs. 9–11). However, some differences were observed for the QQQ and SSS Aβ17–42 V_H domains. The higher binding signals of these domains for disaggregated Aβ in the well plate assay and for fibrils in the immunoblotting assay may be due to the different mechanisms of antigen immobilization and/or the impact of varying antigen concentration (immunoblotting) *versus* varying antibody concentration (well plates). Our findings demonstrate the importance of standardizing assays with well defined fibril and disaggregated peptide samples to properly interpret the results. Indeed, we find that conventional antibodies with conformational specificity for fibrils (LOC and OC) only show fibril specificity at low amounts of immobilized antigen (Fig. 10). Interestingly, we also observe a similar level of conformational specificity for a sequence-specific Aβ antibody (NAB 228) at low amounts of immobilized antigen. This demonstrates that the observed conformational specificity of many antibodies (including conventional ones) is dependent on assay conditions and must be interpreted carefully (65).

A key next step will be to identify the residues within the grafted Aβ17–42 and IAPP8–37 peptides that contribute most to the affinity and conformational specificity of the V_H

domains. This is important to further optimize the antibody domains as well as to guide the design of anti-amyloid antibodies specific for other amyloid-forming polypeptides. We are currently expanding our use of alanine-scanning mutagenesis to the entire CDR3 to identify the most important residues for expression, solubility, and binding. It will also be important to further increase the affinity and conformational specificity of these grafted domains using directed evolution methods. We are currently randomizing positions within and near CDR3 of similar grafted V_H domains, and selecting variants with improved affinity and conformational specificity. We expect that these and related approaches will lead to the rapid design and optimization of antibodies with high conformational and sequence specificity for amyloid aggregates.

Author Contributions—C. C. L and P. M. T. designed the research; C. C. L., M. C. J., K. E. T., F. M., and S. E. D. performed the experiments; R. A. and D. P. R. provided reagents, technical advice, and comments on the manuscript; and C. C. L., M. C. J. and P. M. T. wrote the paper.

Acknowledgments—We thank members of the Tessier lab for their helpful suggestions on our manuscript.

References

1. Chiti, F., and Dobson, C. M. (2006) Protein misfolding, functional amyloid, and human disease. *Annu. Rev. Biochem.* **75,** 333–366
2. Aguzzi, A., and O'Connor, T. (2010) Protein aggregation diseases: pathogenicity and therapeutic perspectives. *Nat. Rev. Drug Discov.* **9,** 237–248
3. Haass, C., and Selkoe, D. J. (2007) Soluble protein oligomers in neurodegeneration: lessons from the Alzheimer's amyloid β-peptide. *Nat. Rev. Mol. Cell Biol.* **8,** 101–112
4. Labbadia, J., and Morimoto, R. I. (2015) The biology of proteostasis in aging and disease. *Annu. Rev. Biochem.* **84,** 435–464
5. Paravastu, A. K., Leapman, R. D., Yau, W. M., and Tycko, R. (2008) Molecular structural basis for polymorphism in Alzheimer's β-amyloid fibrils. *Proc. Natl. Acad. Sci. U.S.A.* **105,** 18349–18354
6. Tycko, R. (2006) Molecular structure of amyloid fibrils: insights from solid-state NMR. *Q. Rev. Biophys.* **39,** 1–55
7. Petkova, A. T., Leapman, R. D., Guo, Z., Yau, W. M., Mattson, M. P., and Tycko, R. (2005) Self-propagating, molecular-level polymorphism in Alzheimer's β-amyloid fibrils. *Science* **307,** 262–265
8. Tycko, R. (2000) Solid-state NMR as a probe of amyloid fibril structure. *Curr. Opin. Chem. Biol.* **4,** 500–506
9. Colvin, M. T., Silvers, R., Frohm, B., Su, Y., Linse, S., and Griffin, R. G. (2015) High resolution structural characterization of Aβ42 amyloid fibrils by magic angle spinning NMR. *J. Am. Chem. Soc.* **137,** 7509–7518
10. Chan, J. C. (2012) Solid-state NMR techniques for the structural determination of amyloid fibrils. *Top. Curr. Chem.* **306,** 47–88
11. Vilar, M., Chou, H. T., Lührs, T., Maji, S. K., Riek-Loher, D., Verel, R., Manning, G., Stahlberg, H., and Riek, R. (2008) The fold of α-synuclein fibrils. *Proc. Natl. Acad. Sci. U.S.A.* **105,** 8637–8642
12. Wasmer, C., Schütz, A., Loquet, A., Buhtz, C., Greenwald, J., Riek, R., Böckmann, A., and Meier, B. H. (2009) The molecular organization of the fungal prion HET-s in its amyloid form. *J. Mol. Biol.* **394,** 119–127
13. Ahmed, M., Davis, J., Aucoin, D., Sato, T., Ahuja, S., Aimoto, S., Elliott, J. I., Van Nostrand, W. E., and Smith, S. O. (2010) Structural conversion of neurotoxic amyloid-β(1–42) oligomers to fibrils. *Nat. Struct. Mol. Biol.* **17,** 561–567
14. Laganowsky, A., Liu, C., Sawaya, M. R., Whitelegge, J. P., Park, J., Zhao, M., Pensalfini, A., Soriaga, A. B., Landau, M., Teng, P. K., Cascio, D., Glabe, C., and Eisenberg, D. (2012) Atomic view of a toxic amyloid small oligomer. *Science* **335,** 1228–1231
15. Sawaya, M. R., Sambashivan, S., Nelson, R., Ivanova, M. I., Sievers, S. A., Apostol, M. I., Thompson, M. J., Balbirnie, M., Wiltzius, J. J., McFarlane, H. T., Madsen, A. Ø., Riekel, C., and Eisenberg, D. (2007) Atomic structures of amyloid cross-β spines reveal varied steric zippers. *Nature* **447,** 453–457
16. Nelson, R., Sawaya, M. R., Balbirnie, M., Madsen, A. Ø., Riekel, C., Grothe, R., and Eisenberg, D. (2005) Structure of the cross-beta spine of amyloid-like fibrils. *Nature* **435,** 773–778
17. Kayed, R., and Glabe, C. G. (2006) Conformation-dependent anti-amyloid oligomer antibodies. *Methods Enzymol.* **413,** 326–344
18. O'Nuallain, B., and Wetzel, R. (2002) Conformational Abs recognizing a generic amyloid fibril epitope. *Proc. Natl. Acad. Sci. U.S.A.* **99,** 1485–1490
19. Kayed, R., Head, E., Sarsoza, F., Saing, T., Cotman, C. W., Necula, M., Margol, L., Wu, J., Breydo, L., Thompson, J. L., Rasool, S., Gurlo, T., Butler, P., and Glabe, C. G. (2007) Fibril specific, conformation dependent antibodies recognize a generic epitope common to amyloid fibrils and fibrillar oligomers that is absent in prefibrillar oligomers. *Mol. Neurodegener.* **2,** 18
20. Kayed, R., Head, E., Thompson, J. L., McIntire, T. M., Milton, S. C., Cotman, C. W., and Glabe, C. G. (2003) Common structure of soluble amyloid oligomers implies common mechanism of pathogenesis. *Science* **300,** 486–489
21. Habicht, G., Haupt, C., Friedrich, R. P., Hortschansky, P., Sachse, C., Meinhardt, J., Wieligmann, K., Gellermann, G. P., Brodhun, M., Götz, J., Halbhuber, K. J., Röcken, C., Horn, U., and Fändrich, M. (2007) Directed selection of a conformational antibody domain that prevents mature amyloid fibril formation by stabilizing Aβ protofibrils. *Proc. Natl. Acad. Sci. U.S.A.* **104,** 19232–19237
22. Morgado, I., Wieligmann, K., Bereza, M., Rönicke, R., Meinhardt, K., Annamalai, K., Baumann, M., Wacker, J., Hortschansky, P., Malešević, M., Parthier, C., Mawrin, C., Schiene-Fischer, C., Reymann, K. G., Stubbs, M. T., Balbach, J., Görlach, M., Horn, U., and Fändrich, M. (2012) Molecular basis of β-amyloid oligomer recognition with a conformational antibody fragment. *Proc. Natl. Acad. Sci. U.S.A.* **109,** 12503–12508
23. Barkhordarian, H., Emadi, S., Schulz, P., and Sierks, M. R. (2006) Isolating recombinant antibodies against specific protein morphologies using atomic force microscopy and phage display technologies. *Protein Eng. Des. Sel.* **19,** 497–502
24. Colby, D. W., Chu, Y., Cassady, J. P., Duennwald, M., Zazulak, H., Webster, J. M., Messer, A., Lindquist, S., Ingram, V. M., and Wittrup, K. D. (2004) Potent inhibition of huntingtin aggregation and cytotoxicity by a disulfide bond-free single-domain intracellular antibody. *Proc. Natl. Acad. Sci. U.S.A.* **101,** 17616–17621
25. Lambert, M. P., Viola, K. L., Chromy, B. A., Chang, L., Morgan, T. E., Yu, J., Venton, D. L., Krafft, G. A., Finch, C. E., and Klein, W. L. (2001) Vaccination with soluble Aβ oligomers generates toxicity-neutralizing antibodies. *J. Neurochem.* **79,** 595–605
26. Vaikath, N. N., Majbour, N. K., Paleologou, K. E., Ardah, M. T., van Dam, E., van de Berg, W. D., Forrest, S. L., Parkkinen, L., Gai, W. P., Hattori, N., Takanashi, M., Lee, S. J., Mann, D. M., Imai, Y., Halliday, G. M., Li, J. Y., and El-Agnaf, O. M. (2015) Generation and characterization of novel conformation-specific monoclonal antibodies for α-synuclein pathology. *Neurobiol. Dis.* **79,** 81–99
27. Vasilevko, V., Pop, V., Kim, H. J., Saing, T., Glabe, C. C., Milton, S., Barrett, E. G., Cotman, C. W., Cribbs, D. H., and Head, E. (2010) Linear and conformation specific antibodies in aged beagles after prolonged vaccination with aggregated Aβ. *Neurobiol. Dis.* **39,** 301–310
28. Lambert, M. P., Velasco, P. T., Viola, K. L., and Klein, W. L. (2009) Targeting generation of antibodies specific to conformational epitopes of amyloid β-derived neurotoxins. *CNS Neurol. Disord. Drug Targets* **8,** 65–81
29. Williamson, R. A., Peretz, D., Pinilla, C., Ball, H., Bastidas, R. B., Rozenshteyn, R., Houghten, R. A., Prusiner, S. B., and Burton, D. R. (1998) Mapping the prion protein using recombinant antibodies. *J. Virol.* **72,** 9413–9418
30. Solomon, B. (2005) Generation of anti-beta-amyloid antibodies via phage display technology towards Alzheimer's disease vaccination. *Vaccine* **23,** 2327–2330
31. Wang, X. P., Zhang, J. H., Wang, Y. J., Feng, Y., Zhang, X., Sun, X. X., Li, J. L., Du, X. T., Lambert, M. P., Yang, S. G., Zhao, M., Klein, W. L., and Liu,

R. T. (2009) Conformation-dependent single-chain variable fragment antibodies specifically recognize β-amyloid oligomers. *FEBS Lett.* **583,** 579–584
32. Lafaye, P., Achour, I., England, P., Duyckaerts, C., and Rougeon, F. (2009) Single-domain antibodies recognize selectively small oligomeric forms of amyloid β, prevent Aβ-induced neurotoxicity and inhibit fibril formation. *Mol. Immunol.* **46,** 695–704
33. Yoshihara, T., Takiguchi, S., Kyuno, A., Tanaka, K., Kuba, S., Hashiguchi, S., Ito, Y., Hashimoto, T., Iwatsubo, T., Tsuyama, S., Nakashima, T., and Sugimura, K. (2008) Immunoreactivity of phage library-derived human single-chain antibodies to amyloid β conformers *in vitro*. *J. Biochem.* **143,** 475–486
34. Droste, P., Frenzel, A., Steinwand, M., Pelat, T., Thullier, P., Hust, M., Lashuel, H., and Dübel, S. (2015) Structural differences of amyloid-β fibrils revealed by antibodies from phage display. *BMC Biotechnol.* **15,** 57
35. Williams, S. M., Venkataraman, L., Tian, H., Khan, G., Harris, B. T., and Sierks, M. R. (2015) Novel atomic force microscopy based biopanning for isolation of morphology specific reagents against TDP-43 variants in amyotrophic lateral sclerosis. *J. Vis. Exp.* 10.3791/52584
36. Yuan, Z., Du, M., Chen, Y., and Dou, F. (2013) Construction of human Fab library and screening of a single-domain antibody of amyloid-β42 oligomers. *Neural Regen. Res.* **8,** 3107–3115
37. Klooster, R., Rutgers, K. S., and van der Maarel, S. M. (2012) Selection of VHH antibody fragments that recognize different Aβ depositions using complex immune libraries. *Methods Mol. Biol.* **911,** 241–253
38. Perchiacca, J. M., Ladiwala, A. R., Bhattacharya, M., and Tessier, P. M. (2012) Structure-based design of conformation- and sequence-specific antibodies against amyloid β. *Proc. Natl. Acad. Sci. U.S.A.* **109,** 84–89
39. Perchiacca, J. M., Lee, C. C., and Tessier, P. M. (2014) Optimal charged mutations in the complementarity-determining regions that prevent domain antibody aggregation are dependent on the antibody scaffold. *Protein Eng. Des. Sel.* **27,** 29–39
40. Perchiacca, J. M., Ladiwala, A. R., Bhattacharya, M., and Tessier, P. M. (2012) Aggregation-resistant domain antibodies engineered with charged mutations near the edges of the complementarity-determining regions. *Protein Eng. Des. Sel.* **25,** 591–601
41. Shivaprasad, S., and Wetzel, R. (2006) Scanning cysteine mutagenesis analysis of Aβ-(1–40) amyloid fibrils. *J. Biol. Chem.* **281,** 993–1000
42. Lührs, T., Ritter, C., Adrian, M., Riek-Loher, D., Bohrmann, B., Döbeli, H., Schubert, D., and Riek, R. (2005) 3D structure of Alzheimer's amyloid-β(1–42) fibrils. *Proc. Natl. Acad. Sci. U.S.A.* **102,** 17342–17347
43. Hoover, D. M., and Lubkowski, J. (2002) DNAWorks: an automated method for designing oligonucleotides for PCR-based gene synthesis. *Nucleic Acids Res.* **30,** e43
44. Studier, F. W. (2005) Protein production by auto-induction in high density shaking cultures. *Protein Expr. Purif.* **41,** 207–234
45. Julian, M. C., Lee, C. C., Tiller, K. E., Rabia, L. A., Day, E. K., Schick, A. J., 3rd, and Tessier, P. M. (2015) Co-evolution of affinity and stability of grafted amyloid-motif domain antibodies. *Protein Eng. Des. Sel.* **28,** 339–350
46. Wilson, D. R., and Finlay, B. B. (1998) Phage display: applications, innovations, and issues in phage and host biology. *Can. J. Microbiol.* **44,** 313–329
47. Miklos, A. E., Kluwe, C., Der, B. S., Pai, S., Sircar, A., Hughes, R. A., Berrondo, M., Xu, J., Codrea, V., Buckley, P. E., Calm, A. M., Welsh, H. S., Warner, C. R., Zacharko, M. A., Carney, J. P., Gray, J. J., Georgiou, G., Kuhlman, B., and Ellington, A. D. (2012) Structure-based design of supercharged, highly thermoresistant antibodies. *Chem. Biol.* **19,** 449–455
48. Bond, C. J., Marsters, J. C., and Sidhu, S. S. (2003) Contributions of CDR3 to VHH domain stability and the design of monobody scaffolds for naive antibody libraries. *J. Mol. Biol.* **332,** 643–655
49. Chang, H. J., Jian, J. W., Hsu, H. J., Lee, Y. C., Chen, H. S., You, J. J., Hou, S. C., Shao, C. Y., Chen, Y. J., Chiu, K. P., Peng, H. P., Lee, K. H., and Yang, A. S. (2014) Loop-sequence features and stability determinants in antibody variable domains by high-throughput experiments. *Structure* **22,** 9–21
50. Perchiacca, J. M., Bhattacharya, M., and Tessier, P. M. (2011) Mutational analysis of domain antibodies reveals aggregation hotspots within and near the complementarity determining regions. *Proteins* **79,** 2637–2647
51. Jaikaran, E. T., Higham, C. E., Serpell, L. C., Zurdo, J., Gross, M., Clark, A., and Fraser, P. E. (2001) Identification of a novel human islet amyloid polypeptide β-sheet domain and factors influencing fibrillogenesis. *J. Mol. Biol.* **308,** 515–525
52. Glenner, G. G., Eanes, E. D., and Wiley, C. A. (1988) Amyloid fibrils formed from a segment of the pancreatic islet amyloid protein. *Biochem. Biophys. Res. Commun.* **155,** 608–614
53. Westermark, P., Engström, U., Johnson, K. H., Westermark, G. T., and Betsholtz, C. (1990) Islet amyloid polypeptide: pinpointing amino acid residues linked to amyloid fibril formation. *Proc. Natl. Acad. Sci. U.S.A.* **87,** 5036–5040
54. Tenidis, K., Waldner, M., Bernhagen, J., Fischle, W., Bergmann, M., Weber, M., Merkle, M. L., Voelter, W., Brunner, H., and Kapurniotu, A. (2000) Identification of a penta- and hexapeptide of islet amyloid polypeptide (IAPP) with amyloidogenic and cytotoxic properties. *J. Mol. Biol.* **295,** 1055–1071
55. Bedrood, S., Li, Y., Isas, J. M., Hegde, B. G., Baxa, U., Haworth, I. S., and Langen, R. (2012) Fibril structure of human islet amyloid polypeptide. *J. Biol. Chem.* **287,** 5235–5241
56. Isas, J. M., Luibl, V., Johnson, L. V., Kayed, R., Wetzel, R., Glabe, C. G., Langen, R., and Chen, J. (2010) Soluble and mature amyloid fibrils in drusen deposits. *Invest. Ophthalmol. Vis. Sci.* **51,** 1304–1310
57. Wu, J. W., Breydo, L., Isas, J. M., Lee, J., Kuznetsov, Y. G., Langen, R., and Glabe, C. (2010) Fibrillar oligomers nucleate the oligomerization of monomeric amyloid β but do not seed fibril formation. *J. Biol. Chem.* **285,** 6071–6079
58. Moroncini, G., Kanu, N., Solforosi, L., Abalos, G., Telling, G. C., Head, M., Ironside, J., Brockes, J. P., Burton, D. R., and Williamson, R. A. (2004) Motif-grafted antibodies containing the replicative interface of cellular PrP are specific for PrPSc. *Proc. Natl. Acad. Sci. U.S.A.* **101,** 10404–10409
59. Heppner, F. L., Musahl, C., Arrighi, I., Klein, M. A., Rülicke, T., Oesch, B., Zinkernagel, R. M., Kalinke, U., and Aguzzi, A. (2001) Prevention of scrapie pathogenesis by transgenic expression of anti-prion protein antibodies. *Science* **294,** 178–182
60. Peretz, D., Williamson, R. A., Kaneko, K., Vergara, J., Leclerc, E., Schmitt-Ulms, G., Mehlhorn, I. R., Legname, G., Wormald, M. R., Rudd, P. M., Dwek, R. A., Burton, D. R., and Prusiner, S. B. (2001) Antibodies inhibit prion propagation and clear cell cultures of prion infectivity. *Nature* **412,** 739–743
61. Enari, M., Flechsig, E., and Weissmann, C. (2001) Scrapie prion protein accumulation by scrapie-infected neuroblastoma cells abrogated by exposure to a prion protein antibody. *Proc. Natl. Acad. Sci. U.S.A.* **98,** 9295–9299
62. Chabry, J., Priola, S. A., Wehrly, K., Nishio, J., Hope, J., and Chesebro, B. (1999) Species-independent inhibition of abnormal prion protein (PrP) formation by a peptide containing a conserved PrP sequence. *J. Virol.* **73,** 6245–6250
63. Chabry, J., Caughey, B., and Chesebro, B. (1998) Specific inhibition of *in vitro* formation of protease-resistant prion protein by synthetic peptides. *J. Biol. Chem.* **273,** 13203–13207
64. Solforosi, L., Bellon, A., Schaller, M., Cruite, J. T., Abalos, G. C., and Williamson, R. A. (2007) Toward molecular dissection of PrPC-PrPSc interactions. *J. Biol. Chem.* **282,** 7465–7471
65. Brännström, K., Lindhagen-Persson, M., Gharibyan, A. L., Iakovleva, I., Vestling, M., Sellin, M. E., Brännström, T., Morozova-Roche, L., Forsgren, L., and Olofsson, A. (2014) A generic method for design of oligomer-specific antibodies. *PLoS ONE* **9,** e90857
66. Baumketner, A., Krone, M. G., and Shea, J. E. (2008) Role of the familial Dutch mutation E22Q in the folding and aggregation of the 15–28 fragment of the Alzheimer amyloid-β protein. *Proc. Natl. Acad. Sci. U.S.A.* **105,** 6027–6032
67. Van Nostrand, W. E., Melchor, J. P., Cho, H. S., Greenberg, S. M., and Rebeck, G. W. (2001) Pathogenic effects of D23N Iowa mutant amyloid β-protein. *J. Biol. Chem.* **276,** 32860–32866
68. Murakami, K., Irie, K., Morimoto, A., Ohigashi, H., Shindo, M., Nagao, M., Shimizu, T., and Shirasawa, T. (2002) Synthesis, aggregation, neurotoxicity, and secondary structure of various Aβ 1–42 mutants of familial Alz-

heimer's disease at positions 21–23. *Biochem. Biophys. Res. Commun.* **294,** 5–10
69. Tycko, R., Sciarretta, K. L., Orgel, J. P., and Meredith, S. C. (2009) Evidence for novel β-sheet structures in Iowa mutant β-amyloid fibrils. *Biochemistry* **48,** 6072–6084
70. Chiti, F., Stefani, M., Taddei, N., Ramponi, G., and Dobson, C. M. (2003) Rationalization of the effects of mutations on peptide and protein aggregation rates. *Nature* **424,** 805–808
71. Yamamoto, N., Hasegawa, K., Matsuzaki, K., Naiki, H., and Yanagisawa, K. (2004) Environment- and mutation-dependent aggregation behavior of Alzheimer amyloid β-protein. *J. Neurochem.* **90,** 62–69
72. Zoghbi, H. Y., and Orr, H. T. (1999) Polyglutamine diseases: protein cleavage and aggregation. *Curr. Opin. Neurobiol.* **9,** 566–570
73. Lu, X., and Murphy, R. M. (2014) Synthesis and disaggregation of asparagine repeat-containing peptides. *J. Pept. Sci.* **20,** 860–867
74. Trevino, S. R., Scholtz, J. M., and Pace, C. N. (2007) Amino acid contribution to protein solubility: Asp, Glu, and Ser contribute more favorably than the other hydrophilic amino acids in RNase Sa. *J. Mol. Biol.* **366,** 449–460
75. Kyte, J., and Doolittle, R. F. (1982) A simple method for displaying the hydropathic character of a protein. *J. Mol. Biol.* **157,** 105–132
76. Sweet, R. M., and Eisenberg, D. (1983) Correlation of sequence hydrophobicities measures similarity in three-dimensional protein structure. *J. Mol. Biol.* **171,** 479–488
77. Wetzel, R. (2012) Physical chemistry of polyglutamine: intriguing tales of a monotonous sequence. *J. Mol. Biol.* **421,** 466–490
78. Ladiwala, A. R., Bhattacharya, M., Perchiacca, J. M., Cao, P., Raleigh, D. P., Abedini, A., Schmidt, A. M., Varkey, J., Langen, R., and Tessier, P. M. (2012) Rational design of potent domain antibody inhibitors of amyloid fibril assembly. *Proc. Natl. Acad. Sci. U.S.A.* **109,** 19965–19970